nature communications

Article | Article in Press

https://doi.org/10.1038/s41467-026-79086-4

Earthquake-driven influx of organic matter enhances authigenic carbonate formation in badal trenches

Received: 10 February 2026

Accepted: 12 October 2026

Published online: 03 November 2026

Check for updates

Yongxin Liu[1,2], Liguo Niu[1,2], Mingzhi Liu[1,2], Renbiao Tao[3] ✉, Chenxin Jing[3], Joel Johnson[4], Li Xu[5], Yong Guan[6], Yubin Hu[7], Min Luo[8], Ken Ikehara[9], Michael Strasser[10] & Rui Bao[1,2] ✉

Shallow marine carbonates are recognized as key agents in deep carbon cycling. However, the formation and burial of carbonates below the carbonate compensation depth still remain poorly understood. Here, we investigate carbonates from the > 7000 m water-depth Japan Trench hadal zone and find widespread authigenic calcium carbonate buried in these ultra-deep sediments. Stable and radiocarbon isotope depletions in the authigenic carbonates indicate an organic carbon (OC) source, likely primarily delivered by deep-sea landslides. Isotopic modeling suggests that subduction of these OC-derived carbonates can impart negative $\delta^{13}C$ signatures to fluids released in the NE Japan subduction zone. The OC-derived carbonate flux in the Japan Trench is estimated to reach ~ 28.6 Tg C Myr^{-1}. We propose that earthquake-driven organic matter influx into the hadal zone may have facilitated sustained carbonate production. Thus, OC-derived authigenic carbonates in hadal trenches represent an underappreciated carbon sink and a potential mechanism for transferring OC into the deep Earth.

Hadal trenches—the deepest manifestations of plate convergence—serve as critical conduits linking Earth's surface to deep material cycles through subducting slabs[1–3]. Frequent seismicity and intense biogeochemical activity characterize these ultra-deep environments, where subducting plates transport vast amounts of carbon-bearing phases (e.g., carbonates) into deep Earth[2,4,5]. This transfer connects the Earth's surface and mantle, governs the recycling of volatiles, and therefore long-term climate evolution and mantle heterogeneity[6,7].

Below the carbonate compensation depth (CCD), where carbonate dissolution exceeds supply, the long-term accumulation of calcareous sediments is generally suppressed. Nevertheless, authigenic carbonate precipitation persists independently of the CCD[7,8], accounting for >10% of global carbonate accumulation in the marine sediments despite dissolution limitations[9]. While global hadal trenches (>6000 m water depth), situated far below the CCD, are largely devoid of carbonates derived from vertically settling phytoplankton and zooplankton, authigenic carbonates have been documented in trench

[1]Frontiers Science Center for Deep Ocean Multispheres and Earth System, and Key Laboratory of Marine Chemistry Theory and Technology, Ministry of Education, Ocean University of China, Qingdao, China. [2]Laboratory for Marine Geology, Qingdao Marine Science and Technology Center, Qingdao, China. [3]Center for High Pressure Science & Technology Advanced Research, Beijing, China. [4]Department of Earth Sciences, University of New Hampshire, Durham, New Hampshire, USA. [5]National Ocean Sciences Accelerator Mass Spectrometry (NOSAMS) Laboratory, Woods Hole Oceanographic Institution, Massachusetts, USA. [6]National Synchrotron Radiation Laboratory, University of Science and Technology of China, Hefei, China. [7]Institute of Marine Science and Technology, Shandong University, Qingdao, China. [8]Shanghai Engineering Research Center of Hadal Science and Technology, College of Marine Sciences, Shanghai Ocean University, Shanghai, China. [9]Institute of Geology and Geoinformation, Geological Survey of Japan, National Institute of Advanced Industrial Science and Technology (AIST), Ibaraki, Japan. [10]Institute of Geology, University of Innsbruck, Innsbruck,, Austria.
✉e-mail: renbiao.tao@hpstar.ac.cn; baorui@ouc.edu.cn

sediments by previous deep-sea expeditions[10] (Supplementary Table 1). Hadal carbonates may thus represent pivotal yet enigmatic players in the deep carbon cycle.

Previous studies mainly focused on the recycling of authigenic carbonates on the shallow-water seafloor[11–14] and found that the deposition of these carbonates is influenced by various environmental factors[11,15–18]. In contrast, the extreme pressure, low temperature, and distinct geochemical regimes below the CCD in hadal settings suggest that the formation pathways and mineral expressions of authigenic carbonates may differ fundamentally from those in shallower marine sediments[10,15,19]. Although sporadic discoveries—such as the occurrence of ikaite in deep-sea settings—point to a potential linkage with organic-matter diagenesis[15,18,20,21], the specific mechanisms, biogeochemical signatures, and micro-environmental controls governing the carbonate precipitation and formation in these ultra-deep oceanic sediments remain poorly understood.

The pronounced spatial heterogeneity in the occurrence of authigenic carbonates raises important questions regarding the limits of organic carbon (OC) supply and the specific conditions that facilitate precipitation beneath the CCD. Additionally, the high-pressure environment of the hadal zone may promote the formation and preservation of carbonate phases that are capable of long-term geological storage, representing a potentially significant yet underexplored pathway for carbon sequestration. However, systematic investigations into their carbon sources, formation triggers, and overall contributions to deep carbon cycling have been limited. Therefore, advancing the study of authigenic carbonates in hadal trenches is crucial not only for understanding their formation mechanisms but also for assessing their role in transferring carbon into the Earth's interior.

Building on evidence that frequent seismic activity in hadal trenches—particularly in the Japan Trench region—triggers landslides that enhance the delivery of OC to these ultra-deep oceanic environments[22,23], we focus our investigation on authigenic carbonate formation under conditions of rapid sediment accumulation. Such high deposition rates provide a compressed temporal archive of deep-sea biogeochemical changes, offering a distinct opportunity to examine carbonate precipitation mechanisms over relatively short timescales.

In this study, we examined carbonate samples from the Japan Trench, collected during International Ocean Discovery Program (IODP) Expedition 386, utilizing an integrated geochemical approach. This approach included synchrotron X-ray mineralogy, energy-dispersive spectrometer (EDS), stepwise acidification, and ramped pyrolysis oxidation (RPO) coupled with ^{13}C and ^{14}C isotope analysis. These methodologies enable us to identify carbon sources, elucidate formation pathways, and trace carbon transfer within carbonates. Our multi-proxy framework quantifies the contributions of earthquake-driven OC to hadal carbonate formation and establishes these authigenic phases in the hadal zone as an important vector in the deep Earth carbon cycle.

Results and discussion

Authigenic carbonate formation in ultra-deep oceanic sediments

We have identified authigenic ikaite and calcite minerals that are widely distributed across various drill holes in the Japan Trench (see Supplementary Table 1 and Supplementary Fig. 1). For instance, carbonate nodules containing a 4 cm authigenic component are observed at Hole M0095[24]. Our analysis focuses on sediments from Hole M0084D, specifically selecting samples from approximately 24.11 meters below the seafloor (mbsf) at M0084D-1H-26, 14–19 cm, which exhibited larger grains (Fig. 1). Notably, we discover translucent amber-colored authigenic carbonates that appear as large grains interspersed with smaller amber grains within the surrounding matrix (detailed lithologies can be found in the Supplementary Information).

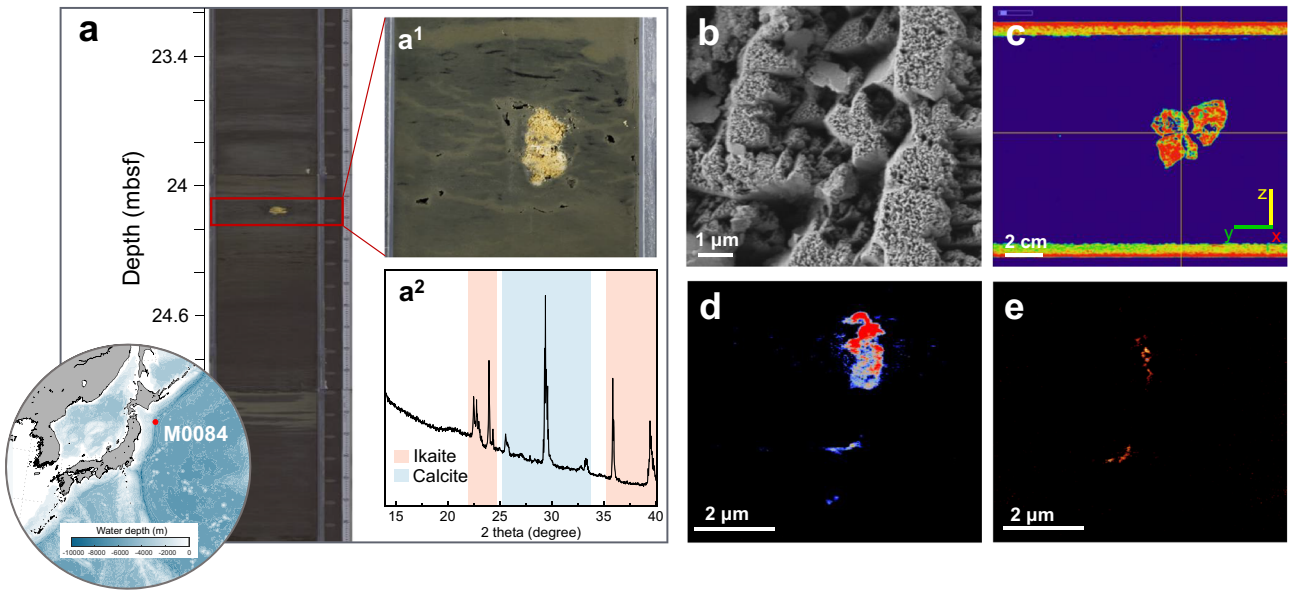


Fig. 1 | Sampling location and characteristics of carbonate minerals in the Japan Trench. a Sampling map indicating the location of Hole M0084D (red dot; 7600 m water depth), along with sediment descriptions and detailed structures observed at depths of 23.2–25.6 m (red box) within Hole M0084D[24]. The map is created with MATLAB. Comprehensive sediment descriptions and detailed structures for M0084D can be found in the Supplementary Materials. Amber-colored authigenic carbonate minerals were identified. In addition to the authigenic carbonate at M0084D-1H-26, 14–19 cm, real photos and scanning electron microscopy (SEM) images of similar carbonates are shown in Supplementary Fig. 1. **a**^{1} Photograph[24] **a**^{2} X-ray diffraction (XRD) spectrum (ikaite-red, calcite-blue) **b** SEM image. **c** Computed tomography (CT) image (side view, x-red) of authigenic carbonate minerals at M0084D-1H-26, 14–19 cm. Additional CT images (top and frontal views) are presented in Supplementary Fig. 2. Synchrotron soft X-ray images: distribution of **d** calcium elements and **e** carbon elements within the authigenic carbonate crystal at M0084D-1H-26, 14–19 cm. The corresponding transmission electron microscopy (TEM) image of the authigenic carbonate crystal is provided in Supplementary Fig. 2.

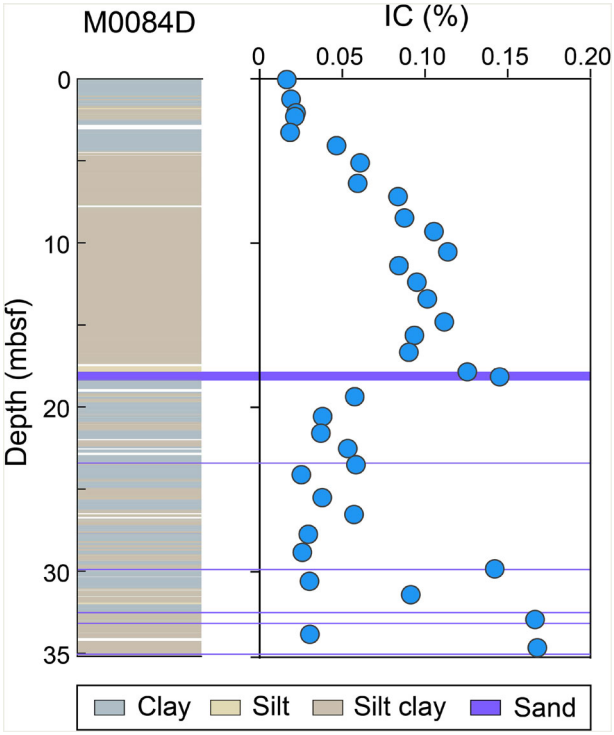


Fig. 2 | Inorganic carbon (IC) content and lithology of the trench sediments. IC content (wt%) and lithology in 0–35 m depth sediments of Hole M0084D. The color blue, brown, yellow and purple represent clay, silty clay, silt, and sand, respectively.

X-ray diffraction (XRD) analysis confirms that these amber-colored authigenic carbonates comprise a mixture of ikaite and calcite (Fig. 1a). The presence of calcite may result from the partial conversion of ikaite to calcite during the sampling process[25]. Additionally, scanning electron microscopy (SEM) images reveal that these granular minerals exhibit a well-defined crystalline structure characterized by rough surfaces, distinct ridges, and steps (Fig. 1b). These clearly defined crystal habits suggest that carbonate growth is controlled by local thermodynamic equilibrium conditions. Our findings indicate that these carbonates originate from in-situ processes within the hadal zone sediments, rather than being the result of biogenic calcium carbonate shells transported from the surface waters due to landslides triggered by external seismic activity. The presence of ikaite, a metastable phase that forms only at near-freezing temperatures, further attests to its in-situ precipitation in the hadal environment.

Inorganic carbon (IC) content in sediments from Hole M0084D, measured at depths of 1–35 m, ranges from 0.02% to 0.17% (average 0.09%, $n = 36$; Fig. 2). This low but persistent IC signal indicates the widespread occurrence of finely disseminated, sub-millimeter authigenic carbonate throughout the sediment column—extending beyond the discrete macroscopic ikaite layer observed at ~24.11 m. Furthermore, elevated bicarbonate derived from active silicate weathering points to authigenic carbonate formation as a dominant sink for released calcium in hadal settings[18]. Our simple machine learning projections model suggest that such precipitation likely continues in deeper, unsampled sediments (see "Methods"). We therefore propose that Japan Trench sediments may represent a previously under-recognized sink for authigenic carbonate.

Photographic and computed tomography (CT) imaging reveals that authigenic carbonate minerals contain internal microfractures and exhibit diffuse grain boundaries, while the surrounding sediment shows abundant voids and pore spaces (Fig. 1a, c and Supplementary Fig. 2). The presence of these cracks may enhance interactions between the minerals and the local porewater environment[15,26], suggesting that localized geochemical conditions adjacent to the minerals —such as those found in interstitial water—could facilitate the formation of additional authigenic carbonates in ultra-deep oceanic sediments. Collectively, our textural observations indicate that large-grained authigenic carbonate deposition in hadal trenches is not controlled by the CCD of the overlying water. It appears to be strongly regulated by in situ, sediment-hosted biogeochemical microenvironments shaped by the distinct tectonic conditions of the deep subseafloor.

Carbon source of deep-oceanic authigenic carbonates

The microenvironment of hadal sediments governs authigenic carbonate formation, which should be reflected in distinct carbon isotopic signatures resulting from the specific carbon sources available during precipitation. To investigate this, we employ stepwise acidification to sequentially separate and analyze the isotopic composition of carbonate from the interior and exterior of authigenic grains. The results show that the carbonate interior is markedly ^{13}C-depleted ($\delta^{13}C = -7.52‰$, faction 2: F_2), in contrast to the exterior ($\delta^{13}C = -2.88‰$, faction 1: F_1; Fig. 3a), indicating the incorporation of isotopically light carbon during initial crystal growth. This light carbon signal is inconsistent with the coexisting porewater dissolved inorganic carbon (DIC), which exhibits a heavy $\delta^{13}C$ value of +10.15‰ (Supplementary Fig. 4)[22]. This stable isotopic disparity between authigenic carbonate and bulk porewater DIC indicates that carbonate precipitation is not inherited from the ambient DIC reservoir. Therefore, the stark isotopic disparity points to a ^{13}C-depleted carbon source —such as dissolved organic carbon (DOC)—for the authigenic carbonate interior.

Synchrotron soft X-ray 3D imaging provides an independent line of evidence that mechanistically links the isotopic signature to a physical location. Conceptually, in a perfect $CaCO_3$ crystal, the IC and calcium maps should be identical. The observed spatial offset—specifically, IC hotspots devoid of calcium signal (Fig. 1d, e and Supplementary Movies 1, 2)—offers a visualization of a discrete, non-lattice carbon phase co-located with the carbonate. This phase is interpreted as the ^{13}C-depleted OC implicated by the isotopic gradient, confirming its incorporation into the growing mineral matrix.

The radiocarbon ages provide further insight into the growth dynamics of authigenic carbonates in ultra-deep oceanic sediments. A distinct ~200-year offset exists between the older interior (5630 ± 25 BP, F_2) and the younger exterior (5450 ± 20 BP, F_1) of the analyzed carbonate grain (Fig. 3a and Supplementary Fig. 5). This age discrepancy—where the core is older than the rim—is consistent with an outward growth model, further indicating that earthquake-driven influx of organic matter may significantly promote the sustained precipitation of authigenic carbonate in hadal sediments.

Notably, both the interior and exterior ages are younger than those of the ambient porewater DOC (~6200 BP) and DIC (~ 6800 BP, Supplementary Fig. 4)[22]. This age relationship, together with the strongly depleted $\delta^{13}C$ values of carbonate relative to porewater DIC, indicates that carbonate does not incorporate carbon simply from the bulk porewater pool. Rather, it likely forms from a younger, more reactive fraction of OC that is selectively mobilized and converted to carbonate during early diagenesis. This growth mechanism directly governs the ultimate source of carbon sequestered in hadal authigenic carbonates, highlighting a preferential pathway for relatively fresh DOC into the mineral phase.

The sedimentary OC adjacent to the authigenic carbonate is markedly younger (3560-4440 years BP) than the carbonate itself. To further resolve the age structure of this OC, we apply the RPO method, which separates OC into four thermal fractions (T_1–T_4: 90–320 °C, 320–391 °C, 391–484 °C, and 484–900 °C). All RPO-derived fractions are likewise younger than the authigenic carbonate (Fig. 3a and

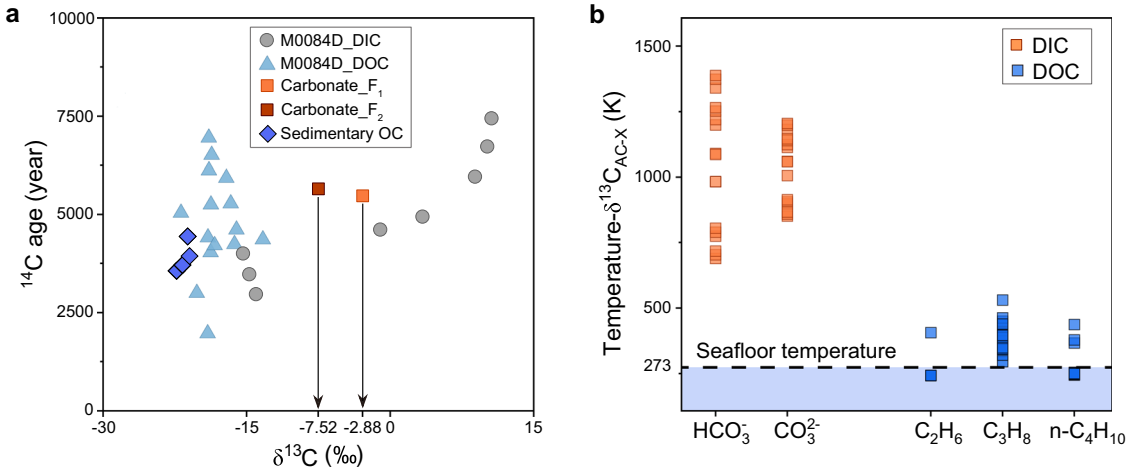


Fig. 3 | Carbon source of authigenic carbonate in the ultra-deep oceanic sediments. a ^{14}C ages and $\delta^{13}C$ values of authigenic carbonate vs. sedimentary organic carbon (OC; blue diamond) at M0084D-1H-26, 14–19 cm, and dissolved organic carbon (DOC; blue triangle) vs. dissolved inorganic carbon (DIC; gray circle) at Hole M0084D. $\delta^{13}C$ values of the authigenic carbonate exterior (Carbonate_F_1; orange square) and interior (Carbonate_F_2; red square) are −2.88‰ and −7.52‰ ("Methods" and Supplementary Fig. 5), respectively. **b** Temperatures of the authigenic carbonate formation in ultra-deep oceanic sediments assuming DIC (HCO_3^-, CO_3^{2-}; orange) or DOC (C_2H_6, C_3H_8, n-C_4H_{10}; blue) is the sole carbon source, respectively. X refers to HCO_3^-, CO_3^{2-}, C_2H_6, C_3H_8, n-C_4H_{10}, respectively. The gray line represents the seafloor temperature (273 K).

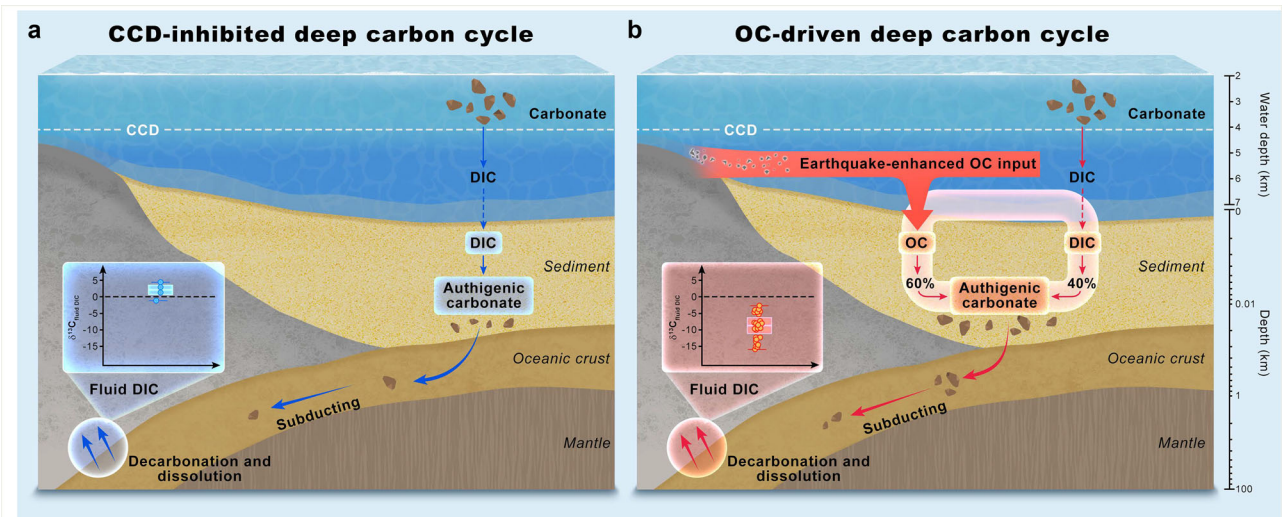


Fig. 4 | Conceptual models of the earthquake-enhanced authigenic carbonate formation in trench sediments and isotope signatures in the subduction zone. The vertically settling phytoplankton and zooplankton dissolve and release dissolved inorganic carbon (DIC) through the carbonate compensation depth (CCD). DIC diffuses into interstitial water in hadal trench sediments. **a** Before seismic events remobilize large masses of organic carbon (OC) into hadal sediments, only the interstitial DIC transforms some microscale authigenic carbonates. During subduction, the carbonates in the trench sediments undergo decarbonation and dissolution, yielding fluid DIC with a heavy $\delta^{13}C$ value, such as ranging from −1‰ to +4‰ (blue), data from ref. 52 **b** Frequent seismic events remobilize large masses of OC into hadal sediments. Earthquake-enhanced OC inputs promote the formation of OC-derived authigenic carbonates, contributing ~60% of the authigenic carbonate carbon; the remaining ~40% of the carbon comes from the overlying water-column DIC and earthquake-enhanced interstitial DIC. Fluid DIC liberated from OC-derived carbonates in hadal trench sediments would have distinctly more $\delta^{13}C$-depleted signatures (−15.7‰ ~ −2.4‰, red).

Supplementary Fig. 3). In addition, these OC fractions exhibit substantially more negative $\delta^{13}C$ values (−22.39‰ to −21.02‰) compared to the interstitial DOC at the same depth (~−18.80‰ at ~24.11 m; Fig. 3a). EDS reveals silicate minerals on authigenic carbonate crystal surfaces (Supplementary Fig. 6), which can adsorb sedimentary OC and thus provide a protected carbon reservoir. Although sedimentary OC is typically less accessible than dissolved carbon due to physical or chemical protection[27], labile fractions—particularly the youngest ^{14}C-enriched components associated with algal- and biopolymer-rich sediments—can be mobilized via diagenesis or directly utilized by microbes[23,28]. This microbial processing likely converts ^{13}C-depleted sedimentary OC into DIC, thereby supporting authigenic carbonate precipitation. While the authigenic carbonate formation in trench sediments is governed by multiple factors[18], earthquake-driven turbidites enhance the production and accumulation of labile DOC in Japan Trench sediments[22]. We propose that the earthquake-driven influx of organic matter promotes the transformation of labile OC into authigenic carbonate in hadal microenvironments. OC-derived carbonate precipitation efficiency is controlled by the influx rate of labile OC, organic matter reactivity, sulfate availability, and methanogenesis rates. While it is difficult to determine the conversion efficiency of earthquake-driven OC to authigenic carbonate in hadal sediments, the OC-derived carbonate precipitation may be widespread across a

north–south transect in the Japan Trench, spanning ~611 km (Supplementary Fig. 7).

To further constrain the carbon source of these authigenic carbonates, we employ a temperature-dependent carbon isotope equilibrium model to estimate their formation temperatures (Y-axis), assuming either DIC (HCO_3^-, CO_3^{2-}) or DOC (C_2H_6, C_3H_8, n-C_4H_{10}) as precursors (Fig. 3b; see "Methods"). The model indicates that when small-molecule DOC is used as the carbon source, the predicted formation temperatures closely align with in situ seafloor conditions. In contrast, using a DIC source yields unrealistically high temperatures that are inconsistent with the hadal environment. These findings provide independent evidence that the carbon in these authigenic carbonates is primarily derived from organic matter. An end-member mixing model based on radiocarbon ages—utilizing sedimentary OC (~3912 years BP), authigenic carbonate (~5540 years BP), porewater DOC (~6200 years BP), and DIC (~ 6800 years BP, Supplementary Fig. 4) as end members—estimates that OC contributes approximately 60% of the carbonate carbon in the analyzed sample. Within this fraction, sedimentary OC accounts for about 46%, as determined by a Monte Carlo simulation (using ^{14}C as a tracer[29], see "Methods").

Earthquake-enhanced OC-derived carbonates precipitation in trench sediments

The high pressure and low temperature conditions found at hadal depths result in an undersaturation of the water column with carbonate, which theoretically prevents in situ precipitation below the CCD[30]. However, the authigenic carbonates observed in the Japan Trench must have formed locally. We propose that their precipitation is facilitated by specific microenvironments within the sediments, where the chemistry of interstitial waters—distinct from that of the overlying seawater—creates localized conditions conducive to carbonate formation. Therefore, our findings—that authigenic carbonates in hadal trenches are predominantly sourced from OC and form in sediment microenvironments below the CCD—require a revision of deep-carbon-cycle models. Importantly, the precipitation and preservation of authigenic carbonates in ultra-deep oceanic sediments are influenced by seismic disturbances.

Several geological observations support our findings. The formation of these carbonates below the CCD reveals a previously overlooked, tectonically enhanced carbon sink. This process is amplified during frequent seismic events (e.g., the 2011 Tohoku-Oki earthquake), which remobilize large masses of OC into hadal trenches[1,23], thereby continuously fueling the authigenic carbonate factory we describe (Fig. 4). The measurable IC content in Japan Trench sediments (0.02–0.17% in the upper 35 m; $n = 36$; Fig. 2) indicates that such precipitation is widespread at the microscale. Notably, the sand layers, which likely represent turbidite event deposits, are enriched in carbonates (Supplementary Fig. 7). Compared with clay-rich sediments, sandy coarse-grained deposits have a lower capacity for OC protection[31]. Therefore, organic matter delivered by event deposits may be more easily degraded, releasing DIC and increasing porewater alkalinity, thereby promoting the precipitation of OC-derived authigenic carbonate in hadal porewater microenvironments. Therefore, the hadal zones with high sedimentation rates and frequent tectonic disturbances may render the coupling process between OC and carbonates more active than on stable continental margins.

The mechanism underlying this earthquake-enhanced carbonate precipitation involves the creation of a localized microenvironment favorable for carbonate growth. Earthquake-enhanced turbidite deposits may generate a more closed porewater microenvironment through rapid burial and instantaneous compaction. Textural evidence supports a model of localized, microenvironment-controlled growth. The internal cracks, diffuse grain boundaries, and surrounding voids observed within the authigenic carbonates and sediment matrix are not passive features. These structures enhance mineral-fluid interactions, facilitating continuous fluid-rock exchange. This creates a self-sustaining feedback mechanism. Initially, carbonate precipitation alters local porosity and permeability, which subsequently influences the diffusion of reactants and concentrates further precipitation in specific microsites[15,26]. Earthquake events may further enhance this non-passive growth model, as the rapid deposition of thick, earthquake-driven sediments over a short period can significantly reduce sediment permeability and rapidly restrict the exchange of porewater with overlying seawater. This mechanism allows the formation of a locally semi-closed microenvironment around carbonates. This confinement prevents the elevated alkalinity generated by OC degradation and AOM from readily diffusing outward, thereby promoting the further growth of microscale authigenic carbonates into large-grained carbonates.

Both the influx of earthquake-driven organic matter and the enrichment of porewater microenvironments are likely to promote OC-derived carbonate formation in deeper trench sediments. This study analyzes the key geochemical parameters of porewater that govern OC-derived carbonate precipitation in hadal microenvironments (see Supplementary Information), using them as predictor variables (alkalinity, Mg^{2+}, Ca^{2+}, pH, methane, methane-to-higher-hydrocarbon ratio, Supplementary Fig. 8) in our machine learning model to quantitatively predict the carbonate precipitation potential in undrilled deeper sediments (Supplementary Fig. 9). We predict the probability distribution of IC content in undrilled sediments across four content intervals (<0.2%, 0.2%–0.25%, 0.25%–0.3%, >0.3%) based on the IODP 386 dataset—collected from 13 sites along the trench-parallel transect spanning over 600 km—and with weights assigned to these six key geochemical parameters (see "Methods"). Extrapolation shows that the probability of IC content exceeding 0.25% increases with sediment depth (34–100 m, Supplementary Fig. 11), implying that OC-derived carbonate formation may further strengthen in undrilled deeper sediments. This suggests that a significant fraction of this carbonate is preserved to greater depths, representing a flux of ~28.6 Tg C Myr^{-1} into the northeastern (NE) Japan subduction zone.

OC-derived carbonates in the deep earth carbon cycle

The distinctive formation pathway of these OC-derived carbonate phases in trench sediments could render them geochemical archives and notably more efficient carriers of major and trace elements into the deep Earth during subduction than OC or pelagic carbonates[32]. The decreased carbonate solubility in cold (e.g., NE Japan) subduction zones could promote carbonate precipitation and drive a net increase in OC-derived carbonate accumulation (<30 km, 0–1 GPa; Supplementary Fig. 13a). After a stage (~30–60 km, 1–2 GPa) during which carbonate precipitation and dissolution may approach dynamic equilibrium, the elevated temperature–pressure conditions and intensified fluid–rock reactions may increase carbonate solubility (>60 km, >2 GPa), thereby promoting the conversion of carbonate carbon into fluid DIC (Supplementary Fig. 15). Their subduction evolution and mineralogical characteristics imply distinct thermodynamic stability and reactivity compared with sedimentary calcite and aragonite. In an alternative case, they may transform into more stable Mg-rich phases (e.g., dolomite, magnesite) in Mg-rich environments and be further transported in the deep Earth through slab subduction[33,34]. Therefore, because of the subduction evolution process and the precipitation from hadal pore fluids, they are likely to incorporate halogens and other trace elements at concentrations reflective of these extreme conditions, potentially serving as distinct records of diagenetic processes in the deepest oceanic realm.

The earthquake-enhanced OC-derived carbonate storage in ultra-deep oceanic sediments may ultimately drive the carbon cycle[14]. The organic origin of these carbonates provides a plausible explanation for the strongly negative $\delta^{13}C$ signatures observed in volcanic CO_2 from certain subduction zones. Globally, the most ^{13}C-depleted arc

emissions are associated with deep trenches[35,36]. We demonstrate that the subduction of the ^{13}C-depleted authigenic carbonates identified here (−7.52‰ to −2.88‰) can directly account for this isotopic signature. Isotopic modeling shows that fluids liberated from such carbonates in the NE Japan subduction zone would have $\delta^{13}C$ values between −15.7‰ and −2.4‰ (Supplementary Fig. 13b)—markedly lower than those of fluids derived from typical pelagic carbonates (~0‰)[37]. This first-order result indicates that hadal authigenic carbonates may have played an important role in driving the negative isotopic bias in arc volcanic emission[38].

Together, our results redefine the mechanisms of carbon transfer in hadal trenches. We establish that authigenic carbonate precipitation below the CCD is not only possible but is fundamentally fueled by OC, creating a direct pathway for organic matter into the ultra-deep oceanic carbon cycle (Fig. 4). This process, governed by hadal microenvironments that are chemically decoupled from the overlying water, challenges the conventional view that the CCD is the ultimate boundary for carbonate-driven subduction. The identification of this mechanism might also reveal a systematic gap in subduction zone carbon inventories. While the precise flux requires further constraint, its potential magnitude—illustrated by our initial estimate of ~28.6 Tg C Myr^{-1} for the NE Japan trench—underscores that carbon cycling at convergent margins is fundamentally controlled by processes within the sediments, independent of the open-ocean seawater chemistry.

Methods

Site description and sampling material

All the piston cores were collected during IODP Expedition 386 in 2021 with a dynamically positioned vessel and a giant piston corer (GPC)[24]. The Holes M0084D (40°23.69′ N, 144°25.27′ E, water depth 7600 m, Fig. 1a), M0083D (38°45.51′ N, 144°07.72′ E, water depth 7627 m), and M0082D (36°06.07′ N, 142°45.37′ E, water depth 8008 m) were collected from the Japan Trench along a north–south transect. The piston cores were scanned by medical computed X-ray tomography (CT)[39], opened and described onboard, where they were stored at 4°C and subsequently sampled. Sub-samples were immediately stored at –20°C before analysis.

Synchrotron soft X-ray 3D images of authigenic carbonate

The synchrotron soft X-ray imaging experiment is performed at the BL07W beamline at the National Synchrotron Radiation Laboratory (NSRL) in Hefei, China. Carbonate samples are re-suspended in Milli-Q water and diluted to the appropriate concentration. A 0.2 μL aliquot of the authigenic carbonate suspension is deposited onto 100-mesh carbon-film copper grids. The grids, containing the carbonate samples, are then transferred to the vacuum cryogenic chamber of the soft X-ray instrument for imaging. Energy bands of 268 eV (pre-L_{III} edge of C), 281 eV (L_{III} edge of C), 340 eV (pre-L_{III} edge of Ca) and 350 eV (L_{III} edge of Ca) are tested, respectively. The carbonate sample on the sample stage is illuminated by the synchrotron soft X-ray illumination using the condenser. After adsorption and scattering by the carbonates, the transmission of the soft X-ray signal is magnified by the 40 nm outermost-zone-width Fresnel zone plate and detected by the charge-coupled device[40].

91 projection images are collected from –45° to + 45° (1° degree intervals) with 30 nm spatial resolution. Then, the optical intensity of the authigenic carbonate at 268 eV is divided by that at 281 eV to obtain the distribution of carbon[41]. The optical intensity of the authigenic carbonate at 340 eV is divided by that at 350 eV to obtain the distribution of calcium. The 3D distribution of carbon and calcium is reconstructed using the total-variation-based simultaneous algebraic reconstruction technique (TV-SART) (Supplementary Movies 1, 2, Fig. 1 and Supplementary Fig. 2c), demonstrating that the distribution of calcium and carbon is concentrated in the regions of strong grayscale.

Isotopic analysis of authigenic carbonate and OC

The ^{14}C ages are measured using the National Ocean Sciences Accelerator Mass Spectrometry Facility (NOSAMS) at Woods Hole Oceanographic Institution. We employ a stepwise acidification method to analyze the ^{14}C ages and $\delta^{13}C$ values of the exterior and interior carbonate[42] (Supplementary Fig. 5). Firstly, the authigenic carbonate sample is reacted by adding H_3PO_4, and the stepwise acidification is divided into two fractions. 39.0 μmol (fraction 1, F_1, the exterior carbonate) and 235.6 μmol (fraction 2, F_2, the interior carbonate) H_3PO_4 are added sequentially to the carbonate and reacted for one hour each time. The evolved gaseous CO_2 is then reduced to graphite for further carbon isotope measurements. $\delta^{13}C$ values are measured by a Finnigan Delta stable isotope ratio mass spectrometer (Oregon State University).

The ^{14}C ages and $\delta^{13}C$ values of sedimentary OC at M0084D-1H-26, 15–17 cm are determined using the RPO method. The samples are freeze-dried, ground, and then 500 mg samples are acidified with 1 M HCl to remove carbonate until no bubbles were present. The samples are rinsed several times with Milli-Q water until the pH reaches neutrality, after which the samples are freeze-dried. 256.6 mg acidified samples are loaded into a quartz reactor and heated uniformly (5 °C min^{-1}) to 900 °C. The gases generated during the heating process are purged isothermally through the chemical reactor. CO_2 samples corresponding to individual thermal fractions are sealed in pre-combusted glass tubes with copper oxide and silver balls for combustion to purify gases before ^{14}C measurement. CO_2 concentrations and thermograms are obtained using a flow-through infrared CO_2 analyzer, divided into four temperature intervals (T_1: 90–320 °C; T_2: 320–391 °C; T_3: 391–484 °C; T_4: 484–900 °C)[23]. Finally, the collected CO_2 from each thermal fraction is tested for ^{14}C and ^{13}C data.

The ^{14}C ages of CO_2 evolve in the different thermal windows increase with increasing temperature, with an extensive range in ages between the lowest (T_1, 3560 ± 20 ^{14}C years) and highest (T_4, 4440 ± 20 ^{14}C years) temperature windows (Fig. 3 and Supplementary Fig. 3). The RPO data show that sedimentary OC at M0084D-1H-26, 15–17 cm is heterogeneous in terms of thermochemical reactivity (Supplementary Fig. 3).

Analysis of IC content in Japan Trench sediments

IC content (wt%) is determined at Ocean University of China using a GasBench-IRMS[43]. 300 μg sediment samples are reacted with 1 mL H_3PO_4 (19.08 mol/L, d = 1.87 g/mL) for six hours, and the gas is collected to analyze IC content by GasBench-IRMS. Based on replicate analyses of IAEA-603, NBS18, and GBW04416 standards, the analytical uncertainty for IC content is within ±10% of the measured values.

Modeling of equilibrium carbon source isotope ($\delta^{13}C$) analysis for authigenic carbonates

Assuming the DOC/DIC is the sole carbon origin of authigenic calcium carbonate (Fig. 3b), the carbon isotope equilibrium temperatures between authigenic carbonate and DIC/DOC are calculated by fitting equations based on theoretically calculated data from ref. 44,45:

$$10^3 \ln\alpha_{CaCO_3-X} = \frac{a}{T^8} \times 10^{24} + \frac{b}{T^6} \times 10^{18} + \frac{c}{T^4} \times 10^{12} + \frac{d}{T^2} \times 10^6 + e \quad (1)$$

We use C_2H_6, C_3H_8 and n-C_4H_{10} to refer to DOC in the interstitial water. X represents HCO_3^-, CO_3^{2-}, C_2H_6, C_3H_8 and n-C_4H_{10}[46], respectively. The fractionation factors of $CaCO_3$ to X are calculated according to Eq. (1) based on the $\delta^{13}C$ values of authigenic carbonate, DIC, and DOC, and the calculated factors (from a to e) are fitted from ref. 46.

Mineralogical characterization of carbonate using XRD and SEM

XRD spectrum is obtained using an in-situ X-ray Diffractometer (Smartlab-9Kw, Japan). The sample is lyophilized and ground into

powder form. The in-situ XRD equipment is pre-cooled before testing. The powder is placed on the glass sample holder of the diffractometer and measured without any temperature control system. XRD measurements of the powder samples are performed at 0.02° intervals, covering a range from 14° to 40° (~14 min). XRD results show that the amber-colored minerals consist of ikaite and calcite. The characteristic peaks at 22.24°, 22.76°, 23.96°, 35.86°, and 39.44° (2θ) represent ikaite peaks, while the peaks at 25.56° and 29.38° (2θ) correspond to the calcite peaks (Fig. 1a). The morphological carbonate is measured using SEM (TESCAN MIRA LMS, China) with gold sprayed onto the sample to enhance the electrical conductivity. Simultaneously, the elemental distribution of authigenic carbonate is analyzed using EDS. EDS mapping shows that the carbonate minerals contained Ca, C, O, and small amounts of Si, Mg, and Al (Supplementary Fig. 6).

Calculation of the carbon contribution for authigenic carbonates

The three end-member model based on a Monte Carlo simulation approach using ^{14}C ages as source marker is employed to distinguish the carbon contribution of sedimentary OC, DOC, and DIC for carbonate in hadal sediments:

$$^{14}C_{carbonate} = f_{sedimentaryOC} \times {}^{14}C_{sedimentary\,OC} + f_{DOC} \times {}^{14}C_{DOC} + f_{DIC} \times {}^{14}C_{DIC} \quad (2)$$

$$f_{sedimentaryOC} + f_{DOC} + f_{DIC} = 1 \quad (3)$$

where the $^{14}C_{sedimentary\ OC}$ is the average ^{14}C age of sedimentary OC (T_1–T_4), $^{14}C_{carbonate}$ is the average ^{14}C age of stepwise acidification carbonate, and the $^{14}C_{DOC}$ and $^{14}C_{DIC}$ ages are from Supplementary Fig. 4, respectively. The Monte Carlo simulation is applied by an IsoSource application[29]. The Monte Carlo simulation is performed with 10,000 iterations, and the mean values of each end-member are the final results.

Predicted IC content in undrilled depth sediments from machine learning modeling

We use sequence-based neural network models, including long short-term memory (LSTM) and gated recurrent unit (GRU) architectures[47,48], to predict the probability distribution of IC content within the undrilled deeper sediments of Hole M0084D (Supplementary Fig. 9).

First, we integrate 28 porewater parameters and IC content collected from 13 Holes along a ~611 km length of the Japan Trench axis to construct the training dataset[24]. We linearly interpolate the measured IC content in the 0–35 m depth sediments to generate an initial continuous IC profile. The input variables include all porewater geochemical parameters and IC content. Then, we formulate the prediction task as a multi-task learning problem, allowing the model to simultaneously learn the depth-dependent variations of all target variables rather than predicting IC independently. The IC data reported in the IODP dataset were calculated as the difference between total carbon (TC) and total organic carbon (TOC), which differs from the analytical method used for our measured IC data[24]. To avoid inconsistencies between the IC dataset of Hole M0084D and those of other Holes caused by methodological differences, all IC data used in this study are taken from the IODP dataset for subsequent modeling.

Second, we divide the dataset into training and test subsets according to depth at a ratio of 9:1 and train the LSTM/GRU models using a fivefold cross-validation strategy (Supplementary Fig. 9). We optimize the models using a weighted mean squared error loss function, in which we assign a higher loss weight to alkalinity, Mg^{2+}, Ca^{2+}, pH, methane, $C_1/(C_2+C_3)$ ratio, and IC content to enhance the sensitivity of the model to the target carbon variable. The trained GRU model outperforms the LSTM model, achieving an average IODP of 0.605 on the test set (Supplementary Table 2), thereby indicating that the sequence-based framework captures the major depth-dependent variability in IC and porewater parameters. This network consists of three GRU layers with 256 hidden units per layer.

Finally, we apply the trained model to predict IC content across the 34–100 m depth of Hole M0084D. To quantify prediction uncertainty, we perform 50 stochastic forward runs to generate probabilistic model outputs and estimate the corresponding uncertainty bounds using Monte Carlo Dropout simulations[49]. This GRU-based multi-task framework provides a data-driven reconstruction of the continuous IC profile. We use a statistical method to calculate the probability distribution of IC content within four content intervals (<0.2%, 0.2–0.25%, 0.25–0.3%, >0.3%) at varying sediment depths (34–40 m, 40–55 m, 55–70 m, 70–85 m, and 85–100 m).

To assess the sensitivity of the prediction model, we conduct a noise-perturbation experiment for Hole M0084D data (Supplementary Fig. 12). We separately add 5% noise to three input groups: IC, six porewater parameters (alkalinity, Mg^{2+}, Ca^{2+}, pH, methane, and $C_1/(C_2+C_3)$ ratio), and other porewater parameters (salinity, NH_4^+, SO_4^{2-}, Na^+, K^+, V, Cu, Zn, Rb, Mo, Cs, Pb, U, Li, B, Si, Mn, Fe, Sr, Ba, Cl^-, and Br^-). During each perturbation experiment, we kept the other input groups unchanged and applied the same trained GRU model without updating model weights. We then compare the perturbed IC prediction with the normal prediction at the 34–100 m sediments to evaluate the robustness of the predicted IC content in undrilled deeper sediments.

Modeling $\delta^{13}C$ evolution of residue carbonates and fluid DIC in subduction zone fluids

The following four-end-member ($CaCO_3$, HCO_3^-, CO_3^{2-} and H_2CO_3) for $\delta^{13}C$ is applied to quantify the $\delta^{13}C$ excursion in subduction zones:

$$\delta^{13}C^{initial}_{CaCO_3} = f_{CaCO_3} \times \delta^{13}C_{CaCO_3} + f_{CO_3^{2-}} \times \delta^{13}C_{CO_3^{2-}} + f_{HCO_3^-} \times \delta^{13}C_{HCO_3^-} + f_{H_2CO_3} \times \delta^{13}C_{H_2CO_3} \quad (4)$$

where $\delta^{13}C^{initial}_{CaCO_3}$ represents $\delta^{13}C$ values of authigenic calcium carbonate (−7.52‰ and −2.88‰, respectively). Firstly, we select the data for HCO_3^-, CO_3^{2-}, and H_2CO_3 from the ref. 32, assuming that 15 g calcium carbonate is dissolved in 1 L of H_2O with an H_2O to mineral ratio of 1:67, and convert the molar mass to obtain the four parameters in Eq. (5).

$$f_{CO_3^{2-}} + f_{HCO_3^-} + f_{H_2CO_3} + f_{CaCO_3} = 1 \quad (5)$$

where f_{CaCO_3}, $f_{HCO_3^-}$, $f_{CO_3^{2-}}$ and f_{H2CO3} represent the molar mass of $CaCO_3$, HCO_3^-, CO_3^{2-} and H_2CO_3, respectively.

Second, we calculate the fractionation factors (a to e) between calcite/aragonite (Cal/Arag) to HCO_3^-, CO_3^{2-} and H_2CO_3 using the basis data from ref. 46. The temperature data are brought into Eq. (4) to get $\Delta^{13}C_{Cal/Arag\text{-}X}$ (X refers to HCO_3^-, CO_3^{2-} and H_2CO_3, respectively). Moreover, the P-T conditions are constrained from 50 °C (0.1 GPa) to 800 °C (2.53 GPa) during the solubility of OC-derived carbonates in subduction zones along an estimated NE Japan subduction zone geotherm based on ref. 50. By substituting Eqs. (4, 5) into Eq. (6), we obtain the $\delta^{13}C$ values of subducted $CaCO_3$, HCO_3^-, CO_3^{2-} and H_2CO_3 in subduction zones (Supplementary Fig. 13b and Supplementary Fig. 14):

$$\Delta^{13}C_{Cal/Arag-X} = 10^3 ln\alpha_{Cal/Arag-X} = \frac{a}{T^8} \times 10^{24} + \frac{b}{T^6} \times 10^{18} + \frac{c}{T^4} \times 10^{12} + \frac{d}{T^2} \times 10^6 + e \quad (6)$$

Then, the $\delta^{13}C$ of fluid DIC is calculated from $\delta^{13}C$ of HCO_3^-, CO_3^{2-}, and H_2CO_3 based on the dissolution rate of these three carbon-bearing species in ref. 32.

Flux estimation for OC-derived carbonate C in subduction zones

The influx of carbonate C in the NE Japan subduction zone is estimated by multiplying the convergence velocity (8.5 cm/yr[28]), trench length (800 km[1]), sediment thickness (estimated 1000 m), sediment density (0.6 g/cm^3), and average IC content (0.07 wt%, 0–35 m) using the calculation method from ref. 51. The sediment density (dry density, g/cm^3) was measured by gamma-ray attenuation density analyses (Geotek MSCL)[39].

Data availability

The datasets generated and analysed in this study are provided in the Supplementary Information and Source Data file. They are also available from the Figshare repository at https://doi.org/10.6084/m9.figshare.30702749. Source data are provided with this paper.

Code availability

The code generated and used for data processing, analysis, and visualization in this study is available from the Figshare repository at https://doi.org/10.6084/m9.figshare.30702749.

References

1. Kioka, A. et al. Megathrust earthquake drives drastic organic carbon supply to the hadal trench. *Sci. Rep.* **9**, 1553 (2019).
2. Stern, R. J. et al. Subduction zones. *Rev. Geophys.* **40**, 3-1–3-38 (2002).
3. Kioka, A. et al. Event Stratigraphy in a Hadal Oceanic Trench: The Japan Trench as Sedimentary Archive Recording Recurrent Giant Subduction Zone Earthquakes and Their Role in Organic Carbon Export to the Deep Sea. *Front. Earth Sci.* **7**, 319 (2019).
4. Schauberger, C. et al. Microbial community structure in hadal sediments: high similarity along trench axes and strong changes along redox gradients. *ISME J.* **15**, 3455–3467 (2021).
5. Berner, R. A. The long-term carbon cycle, fossil fuels and atmospheric composition. *Nature* **426**, 323–326 (2003).
6. Spandler, C. & Pirard, C. Element recycling from subducting slabs to arc crust: A review. *Lithos* **170**, 208–223 (2013).
7. Turchyn, A. V., Bradbury, H. J., Walker, K. & Sun, X. Controls on the precipitation of carbonate minerals within marine sediments. *Front. Earth Sci.* **9**, 618311 (2021).
8. Zhang, H., Zhou, X., Jiang, X., Hernández-Almeida, I. & Liu, C. The source of Pleistocene carbonate below the CCD in the central basin of the South China Sea: evidences from coccolith and geochemistry. *Mar. Geol.* **457**, 107011 (2023).
9. Sun, X. L. & Turchyn, A. Significant contribution of authigenic carbonate to marine carbon burial. *Nat. Geosci.* **7**, 201–204 (2014).
10. Wefer, G. Report and preliminary results of R/V SONNE Cruise SO219A, Tohoku-Oki-Earthquake-Japan Trench, Yokohama-Yokohama, 08.03.2012-06.04.2012. **301** (2014).
11. Torres, M. E. et al. Silicate weathering in anoxic marine sediment as a requirement for authigenic carbonate burial. *Earth Sci. Rev.* **200**, 102960 (2020).
12. Peckmann, J. & Thiel, V. Carbon cycling at ancient methane–seeps. *Chem. Geol.* **205**, 443–467 (2004).
13. Kelemen, P. B. & Manning, C. E. Reevaluating carbon fluxes in subduction zones: what goes down, mostly comes up. *PNAS* **112**, E3997–E4006 (2015).
14. Plank, T. & Manning, C. E. Subducting carbon. *Nature* **574**, 343–352 (2019).
15. Zabel, M. & Schulz, H. D. Importance of submarine landslides for non-steady state conditions in pore water systems- Lower Zaire (Congo) deep-sea fan. *Mar. Geol.* **176**, 87–99 (2001).
16. Hu, Y. B., Wolthers, M., Wolf-Gladrow, D. A. & Nehrke, G. Effect of pH and phosphate on calcium carbonate polymorphs precipitated at near-freezing temperature. *Cryst. Growth Des.* **15**, 1596–1601 (2015).
17. Moras, C. A., Bach, L. T., Cyronak, T., Joannes-Boyau, R. & Schulz, K. G. Ocean alkalinity enhancement–avoiding runaway $CaCO_3$ precipitation during quick and hydrated lime dissolution. *Biogeosciences* **19**, 3537–3557 (2022).
18. Luo, M. et al. Rapid burial and intense degradation of organic matter drive active silicate weathering in the subsurface sediments of the ocean's deepest realm. *Geology* **53**, 636–641 (2025).
19. Ito, T. Ikaite from cold spring water at Shiowakka, Hokkaido, Japan. *J. Mineral. Petrol. Econ. Geol.* **91**, 209–219 (1996).
20. Zhao, M.-Y., Zheng, Y.-F. & Zhao, Y.-Y. Seeking a geochemical identifier for authigenic carbonate. *Nat. Commun.* **7**, 10885 (2016).
21. Mazzullo, S. J. Organogenic dolomitization in peritidal to deep-sea sediments. *J. Sediment. Res.* **70**, 10–23 (2000).
22. Chu, M. et al. Earthquake-enhanced dissolved carbon cycles in ultra-deep ocean sediments. *Nat. Commun.* **14**, 5427–5427 (2023).
23. Bao, R. et al. Tectonically-triggered sediment and carbon export to the Hadal zone. *Nat. Commun.* **9**, 121 (2018).
24. Strasser, M. et al. Expedition 386 summary. In: Japan Trench Paleoseismology (2023).
25. Hiruta, A. & Matsumoto, R. Geochemical comparison of ikaite and methane-derived authigenic carbonates recovered from Echigo Bank in the Sea of Japan. *Mar. Geol.* **443**, 106672 (2022).
26. Ritger, S., Carson, B. & Suess, E. Methane-derived authigenic carbonates formed by subduction-induced pore-water expulsion along the Oregon/Washington margin. *Geol. Soc. Am. Bull.* **98**, 147–156 (1987).
27. Burdige, D. J. Preservation of organic matter in marine sediments: controls, mechanisms, and an imbalance in sediment organic carbon budgets? *Chem Rev.* **107**, 467–485 (2007).
28. Schwestermann, T. et al. Event-dominated transport, provenance, and burial of organic carbon in the Japan Trench. *Earth Planet. Sci. Lett.* **563**, 116870 (2021).
29. Andersson, A. A systematic examination of a random sampling strategy for source apportionment calculations. *Sci. Total Environ.* **412-413**, 232–238 (2011).
30. Sulpis, O., Jeansson, E., Dinauer, A., Lauvset, S. K. & Middelburg, J. J. Calcium carbonate dissolution patterns in the ocean. *Nat. Geosci.* **14**, 423–428 (2021).
31. Bergamaschi, B. A. et al. The effect of grain size and surface area on organic matter, lignin and carbohydrate concentration, and molecular compositions in Peru Margin sediments. *Geochim. Cosmochim. Acta* **61**, 1247–1260 (1997).
32. Errázuriz-Henao, C. et al. Generation of carbonated peridotite melts via biogenic sediment recycling in modern subduction zones. *Sci. Adv.* **12**, eaec1599 (2026).
33. Wang, S.-J. & Li, S.-G. Magnesium isotope geochemistry of the carbonate-silicate system in subduction zones. *Natl. Sci. Rev.* **9**, nwac036 (2022).
34. Lan, C., Tao, R., Huang, F., Jiang, R. & Zhang, L. High-pressure experimental and thermodynamic constraints on the solubility of carbonates in subduction zone fluids. *Earth Planet. Sci. Lett.* **603**, 117989 (2023).
35. Edmond, J. M. & Huh, Y. Non-steady-state carbonate recycling and implications for the evolution of atmospheric PCO_2. *Earth Planet. Sci. Lett.* **216**, 125–139 (2003).
36. Mason, E., Edmonds, M. & Turchyn, A. V. Remobilization of crustal carbon may dominate volcanic arc emissions. *Science* **357**, 290–294 (2017).
37. Morse, J. W. & Mackenzie, F. T. Geochemistry of sedimentary carbonates. (Elsevier, 1990).
38. Tumiati, S. et al. Subducted organic matter buffered by marine carbonate rules the carbon isotopic signature of arc emissions. *Nat. Commun.* **13**, 2909 (2022).
39. Strasser, M. et al. Expedition 386 methods. In: *Japan Trench Paleoseismology* (2023).

40. Zhang, C. et al. On-line fluorescence microscopy for identification and imaging of apoptotic cell with synchrotron-based soft X-ray tomography. *Micromachines* **14**, 326 (2023).
41. Ding, J. et al. Single-particle analysis for structure and iron chemistry of atmospheric particulate matter. *Anal. Chem.* **92**, 975–982 (2020).
42. Beaupré, S. R., Roberts, M. L., Burton, J. R. & Summons, R. E. Rapid, high-resolution ^{14}C chronology of ooids. *Geochim. Cosmochim. Acta* **159**, 126–138 (2015).
43. Wang, N., Zhao, Y. & Tian, Y. Influences of acid fractionation on determination of carbon and oxygen isotope analysis of carbonates using gasbench-IRMS. *J. Chin. Mass Spectrom. Soc.* **45**, 401–411 (2024).
44. Horita, J. Carbon isotope exchange in the system CO_2-CH_4 at elevated temperatures. *Geochim. Cosmochim. Acta* **65**, 1907–1919 (2001).
45. Richet, P., Bottinga, Y. & Javoy, M. A review of hydrogen, carbon, nitrogen, oxygen, sulphur, and chlorine stable isotope fractionation among gaseous molecules. *Annu. Rev. Earth Planet. Sci.* **5**, 65–110 (1977).
46. Chacko, T., Cole, D. R. & Horita, J. Equilibrium oxygen, hydrogen and carbon isotope fractionation factors applicable to geologic systems. *Rev. Mineral. Geochem.* **43**, 1–81 (2001).
47. Cho, K. et al. Learning Phrase Representations using RNN Encoder–Decoder for Statistical Machine Translation. In *Proceedings of the 2014 Conference on Empirical Methods in Natural Language Processing (EMNLP)* 1724–1734 (Association for Computational Linguistics, Doha, 2014).
48. Hochreiter, S. & Schmidhuber, J. Long short-term memory. *Neural Comput* **9**, 1735–1780 (1997).
49. Gal, Y. & Ghahramani, Z. Dropout as a Bayesian approximation: insights and applications. *International Conference on Machine Learning*, 1050–1059 (2016).
50. Oyanagi, R. & Okamoto, A. Subducted carbon weakens the forearc mantle wedge in a warm subduction zone. *Nat. Commun.* **15**, 7159 (2024).
51. Li, L. & Bebout, G. E. Carbon and nitrogen geochemistry of sediments in the Central American convergent margin: insights regarding subduction input fluxes, diagenesis, and paleoproductivity. *J. Geophys. Res. Solid Earth* **110**, B11202 (2005).
52. Albers, E. et al. Fluid–rock interactions in the shallow Mariana forearc: carbon cycling and redox conditions. *Solid Earth* **10**, 907–930 (2019).

Acknowledgments

We thank the IODP for providing samples and data for this research. We greatly appreciate the assistance of staff from NOSAMS and Ocean University of China in all aspects of the carbon isotopic measurements. We are also grateful to Matthieu Galvez for his constructive comments on this manuscript.

Author contributions

R.B. conceived the experimental study, wrote the manuscript and is responsible for data analysis. All members of the IODP 386 Science Party contributed to sample acquirement, geochemical analysis and data collection. Y.L., R.B., L.X., and Y.G. conducted sample measurements. Y.L., R.B., R.T., C.J., L.N., and M.L. conducted data visualization and prediction model. Y.L., R.B., M.L., R.T., C.J., M.S., K.I., Y.G., J.J., M.L., and Y.H. contributed to the interpretation of data and the editing of the manuscript.

Funding

This study is supported by National Natural Science Foundation of China (Grant: 42525604, 42450135, R.B.), National Key R&D Program of China (Grant: 2025YFF0516900 & 2025YFF0516903, R.B.), National Natural Science Foundation of China (Grant: 92158206, R.T.; 12375330, Y.G.), and Fundamental Research Funds for the Central Universities (Grant: 202042010, R.B.). The collection of synchrotron soft X-ray images is supported by the National Synchrotron Radiation Laboratory of China (Grant: 2021-HLS-PT-004040, R.B.).

Competing interests

The authors declare no competing interests.

Additional information

Supplementary information The online version contains supplementary material available at https://doi.org/10.1038/s41467-026-79086-4.

Correspondence and requests for materials should be addressed to Renbiao Tao or Rui Bao.

Peer review information *Nature Communications* thanks Chao Li and the other, anonymous reviewer(s) for their contribution to the peer review of this work. A peer review file is available.

Reprints and permissions information is available at http://www.nature.com/reprints

Publisher's note Springer Nature remains neutral with regard to jurisdictional claims in published maps and institutional affiliations.

Open Access This article is licensed under a Creative Commons Attribution-NonCommercial-NoDerivatives 4.0 International License, which permits any non-commercial use, sharing, distribution and reproduction in any medium or format, as long as you give appropriate credit to the original author(s) and the source, provide a link to the Creative Commons licence, and indicate if you modified the licensed material. You do not have permission under this licence to share adapted material derived from this article or parts of it. The images or other third party material in this article are included in the article's Creative Commons licence, unless indicated otherwise in a credit line to the material. If material is not included in the article's Creative Commons licence and your intended use is not permitted by statutory regulation or exceeds the permitted use, you will need to obtain permission directly from the copyright holder. To view a copy of this licence, visit http://creativecommons.org/licenses/by-nc-nd/4.0/.

© The Author(s) 2026

This Article in Press is shared early to give you faster access to new research. It is citable and carries a permanent DOI. The final edited version will replace it automatically.